Role of the neck degree of freedom in cold fusion reactions

G. G. Adamian,[1] N. V. Antonenko,[1] and H. Lenske[2]
[1]*Joint Institute for Nuclear Research, Dubna 141980, Russia*
[2]*Institut für Theoretische Physik der Justus–Liebig–Universität, D-35392 Giessen, Germany*
(Received 9 March 2015; published 5 May 2015)

Mass parameters for collective variables of dinuclear systems formed in cold fusion reactions are microscopically calculated with the linear response theory making use of the width of single-particle states and the fluctuation-dissipation theorem. The single-particle spectrum and potential energy surface of the adiabatic two-center shell model are used. The microscopical mass parameter in the neck is found to be much larger than one obtained with the hydrodynamical model. Therefore, the dinuclear system lives a rather long time, comparable to the characteristic time of fusion and, correspondingly, the fusion can be considered at fixed neck parameter. With an adiabatic melting of the dinuclear system along the internuclear distance into a compound system one cannot explain the experimental trends in cold fusion reactions.

DOI: 10.1103/PhysRevC.91.054602 PACS number(s): 25.70.Jj, 24.10.−i, 24.60.−k

I. INTRODUCTION

The synthesis of superheavy nuclei [1,2] and the production of strongly deformed nuclear states [3] stimulate the study of the process of complete fusion in heavy ion collisions at energies near the Coulomb barrier. The initial stage of the fusion of heavy ions is characterized by the formation of a dinuclear system (DNS) when a significant part of the kinetic energy is transferred into the internal excitation energy. The further evolution of the DNS predetermines the process of compound nucleus formation or quasifission (the DNS decay). To describe the evolution of the DNS in collective coordinates, namely in the distance R between the centers of colliding nuclei (or relative elongation λ of the system), the mass and charge asymmetry degrees of freedom $\eta = (A_1 - A_2)/A$ and $\eta_Z = (Z_1 - Z_2)/Z$, respectively, (A_1, A_2 and Z_1, Z_2 are mass and charge numbers of the nuclei, $A = A_1 + A_2$, $Z = Z_1 + Z_2$), the parameter ε of the neck and deformation coordinates of nuclei [4–12], the dissipative, conservative, and inertial forces for these variables have to be determined.

The existing fusion models are distinguished by the choice of the relevant collective variables along which the fusion mainly occurs. While the approaches based on the macroscopic dynamical model [8] the fusion in R at almost fixed value of η, the DNS model [10,13–17] considers the DNS evolution in mass asymmetry by nucleon or cluster transfers as the main path to the compound nucleus. The DNS model assumes basically that the neck degree of freedom is almost fixed in the evolution in η and the nuclei are hindered to melt together by a variation in the relative distance. As shown in Refs. [16–20], this occurs due to the relatively large inertia of the neck degree of freedom and structural forbiddenness effects. In this paper we study dynamical restrictions for the growth of the neck in the DNS with microscopically calculated DNS inertia tensor in the cold fusion reactions.

There are various macroscopical and microscopical approaches to calculate the inertia tensor [21–23]. The macroscopical approaches (see, for example, [8,12,23]) are based on the hydrodynamical model of the nucleus. A calculation of the inertia tensor with a theory for quantum fluid dynamics is suggested in Ref. [24]. By using a random-matrix model to describe the coupling between a collective nuclear variable and intrinsic degrees of freedom and applying the functional integral approach, mass parameters are derived in Ref. [25]. In the linear response theory [26,27] the inertia tensor is found for fissioning nuclei. The microscopical approaches mainly use the cranking type expression and perform calculations in different single-particle bases applying adiabatic [6,7,28–30] or diabatic [31] two-center shell models. The importance of microscopical mass coefficients in describing the spontaneous fission half-life for superheavy nuclei is stressed in Ref. [30]. Difficulties in the cranking-type calculations arise for collective motions with large amplitudes, for example, in fusion or fission, due to pseudocrossings or crossings of levels in the single-particle spectrum. Disregard the contributions from the crossings (pseudocrossings) which means a neglect of effects of configuration changes on the mass parameters during the evolution of the nuclear shape in spite of the fact that the collective inertia is strongly influenced by level crossings (pseudocrossings) [32,33]. In order to overcome this problem, two-body collisions should be incorporated through a width of the single-particle levels and an effective reduction of the level crossing effects. For example, calculations of the nuclear inertia in a generalized cranking model with pairing correlations yielded masses of about one order of magnitude larger than the ones without pairing [34].

One of the aims of the paper is to present analytical expressions for mass parameters using the microscopical methods with residual interaction effects. In Sec. II the mass parameters are obtained within the linear response theory taking the fluctuation-dissipation theorem and the width of single-particle states into consideration. In Sec. III the mass parameters for the relevant collective variables (elongation and neck) of the system formed in cold fusion reactions are evaluated in the two-center shell model with adiabatic basis. The complete fusion process is discussed in adiabatic limit and the diabatic effects are considered. Sec. IV contains a short summary.

II. MICROSCOPICAL MASS COEFFICIENTS

Let us consider a nuclear system described by a single collective coordinate Q and intrinsic single-particle coordinates

x_i (with the conjugated momentum p_i). By expanding the Hamiltonian $H(x_i, p_i, Q)$ to the second order in the vicinity of Q_0, we describe a collective motion within a locally harmonic approximation:

$$H(x_i,p_i,Q) = H(x_i,p_i,Q_0) + (Q-Q_0)F(x_i,p_i,Q_0) + \frac{1}{2}(Q-Q_0)^2\left\langle\frac{\partial^2 H(x_i,p_i,Q)}{\partial Q^2}\right\rangle_{Q_0,T_0}. \quad (1)$$

The coupling term between the collective and intrinsic motion is proportional to the first order in $(Q - Q_0)$ with an operator F given by the derivative of the mean field with respect to Q in the neighborhood of Q_0.

The local motion in Q is described in terms of the collective response function $\chi_{\rm coll}$ of the Q mode. By applying the linear response theory [26,35], the Fourier transform of this function is defined as

$$\chi_{\rm coll}(\omega) = \frac{k^2\chi(\omega)}{1+k\chi(\omega)}, \quad (2)$$

where $\chi(\omega)$ is the Fourier transform of the response function for intrinsic motion which measures how, at some given Q_0 and temperature T_0, the nucleonic degrees of freedom (x_i, p_i) react to the coupling with collective motion. The coupling constant k is then written in the form

$$-k^{-1} = \left\langle\frac{\partial^2\hat{H}(x_i,p_i,Q)}{\partial Q^2}\right\rangle_{Q_0,T_0} = \frac{\partial^2 E(Q,S_0)}{\partial Q^2}|_{Q_0} + \chi(\omega=0) = C(0)+\chi(0) \quad (3)$$

with $\chi(0)$ and $C(0)$ being the static intrinsic response and stiffness, respectively. Because the constant k is entirely determined by quasistatic properties, E is the internal energy at a given entropy S_0 or the free energy at a given temperature T_0. The structure of Eq. (3) reflects the self-consistency between the treatment of collective and microscopic dynamics. It expresses the response of the system of interacting nucleons in terms of the response of the individual nucleons. Note that our application of linear response theory goes along the assumption that the collective motion is slow compared to the dynamics of the nucleons.

In general the frequency dependence of $\chi_{\rm coll}(\omega)$ exhibits a complex structure and shows individual peaks. They may be interpreted to represent individual modes of the nuclear system. For each one may then define the transport coefficients for average motion, namely, mass M, friction γ, stiffness C coefficients, by identifying for the corresponding range of frequencies an oscillator response function

$$\chi_{\rm osc}(\omega) = [-M\omega^2 - \gamma i\omega + C]^{-1}. \quad (4)$$

Replacing $\chi_{\rm coll}(\omega)$ by $\chi_{\rm osc}(\omega)$ from Eq. (4) and employing Eq. (2), we obtain the following expression for the mass coefficient [26,27,35,36]:

$$M = -\frac{1}{2}\frac{\partial^2}{\partial\omega^2}\frac{1}{\chi_{\rm osc}(\omega)}\bigg|_{\omega=0} = \frac{1}{2k^2}\frac{\partial^2}{\partial\omega^2}\frac{1}{\chi(\omega)}\bigg|_{\omega=0} = \left(1+\frac{C(0)}{\chi(0)}\right)^2\left[M^{\rm cr}+\frac{\gamma^2(0)}{\chi(0)}\right], \quad (5)$$

where

$$M^{\rm cr} = \frac{1}{2}\frac{\partial^2\chi(\omega)}{\partial\omega^2}\bigg|_{\omega=0} \quad (6)$$

is the inertia in the zero-frequency limit of the second derivative of the intrinsic response function. $M^{\rm cr}$ can be shown to be similar to the one of the cranking model. For many applications, the value of $C(0)/\chi(0)$ is much less than unity. However, the additional term $\gamma^2(0)/\chi(0)$ in Eq. (5) gives a positive contribution to M where $\gamma(0)$ is the friction coefficient defined by

$$\gamma(0) = -i\left.\frac{\partial\chi(\omega)}{\partial\omega}\right|_{\omega=0} = \left.\frac{\partial\chi''(\omega)}{\partial\omega}\right|_{\omega=0} = \frac{1}{2T_0}\psi''(0). \quad (7)$$

The dissipative part of the response function $\chi''(\omega)$ is connected with the dissipative part of the correlation function $\psi''(\omega)$ through the fluctuation-dissipation theorem:

$$\chi''(\omega) = \frac{1}{\hbar}\tanh\left(\frac{\hbar\omega}{2T_0}\right)\psi''(\omega). \quad (8)$$

The $\psi''(\omega)$ has a singularity of δ-function type at $\omega = 0$:

$$\psi''(\omega) = 2\pi\psi^0\delta(\omega) + \psi''_R(\omega) \quad (9)$$

with $\psi''_R(\omega)$ being regular at $\omega = 0$. In the case of an independent particle model we have

$$\psi''(\omega) = \pi\hbar\sum_{j,k}|F_{jk}|^2 n(e_j)[1-n(e_k)] \times[\delta(\hbar\omega - e_{kj}) + \delta(\hbar\omega + e_{kj})]. \quad (10)$$

Here, $e_{kj} = e_k - e_j$ is the difference of single-particle energies calculated with respect to a Fermi energy, $n(e_j)$ are the occupation numbers, and $F_{jk} = \langle j|F|k\rangle$ the single-particle matrix elements of the operator F. At $j = k$ and $\omega = 0$ we find the contributions from the diagonal matrix elements:

$$\psi^0 = \sum_k |F_{kk}|^2 n(e_k)[1-n(e_k)] = T_0\sum_k\left|\frac{\partial n(e)}{\partial e}\right|_{e=e_k}\left(\frac{\partial e_k}{\partial Q}\right)^2. \quad (11)$$

The last part in Eq. (11) was derived with a Fermi distribution for the occupation numbers, which is characterized by the temperature T_0. The value of T_0 does not effectively go to zero with decreasing excitation energy because each single-particle level has a width due to the two-body interaction. Indeed at zero excitation energy the distribution of the occupation numbers deviates from a step function at least due to pairing correlations. If we replace the δ functions in Eq. (9) or (10), we have to apply Lorentzian functions with the double single-particle width 2Γ, where Γ is the single-particle width, because $\hbar\omega$ is the transition energy between two single-particle states [26]. Therefore, we substitute the δ functions in Eq. (10) by $\Gamma/[\pi((\hbar\omega \pm e_{kj})^2 + \Gamma^2)]$. Then using Eqs. (7)–(11), we can write the friction coefficient in the following form:

$$\gamma(0) = \gamma^{\rm diag}(0) + \gamma^{\rm nondiag}(0), \quad (12)$$

where

$$\gamma^{\rm diag}(0) = \frac{\hbar}{\Gamma}\sum_k \left|\frac{\partial n(e)}{\partial e}\right|_{e=e_k}\left(\frac{\partial e_k}{\partial Q}\right)^2. \quad (13)$$

For smaller temperatures $T_0 < 1.5$ MeV which are of interest here, $\gamma^{\rm diag}(0)$ is much larger than $\gamma^{\rm nondiag}(0)$ [26]. The static response is found as

$$\begin{aligned}\chi(0) &= \lim_{\epsilon\to 0}\int_{-\infty}^{+\infty}\frac{d\omega}{\pi}\frac{\chi''(\omega)}{\omega - i\epsilon}\\ &= \lim_{\epsilon\to 0}\int_{-\infty}^{+\infty}\frac{d\omega}{\hbar\pi}\frac{\tanh\left(\frac{\hbar\omega}{2T_0}\right)\psi''(\omega)}{\omega - i\epsilon}\\ &= \chi^{\rm diag}(0) + \chi^{\rm nondiag}(0), \end{aligned} \quad (14)$$

where

$$\chi^{\rm diag}(0) = \sum_k \left|\frac{\partial n(e)}{\partial e}\right|_{e=e_k}\left(\frac{\partial e_k}{\partial Q}\right)^2. \quad (15)$$

With realistic assumptions $\gamma^{\rm diag}(0) \gg \gamma^{\rm nondiag}(0)$ and $\chi^{\rm diag}(0) \gg \chi^{\rm nondiag}(0)$ and neglecting $C(0)/\chi(0)$, we can divide the mass parameter (5) as

$$M = M^{\rm diag} + M^{\rm nondiag}. \quad (16)$$

The contribution of the diagonal matrix elements of F to M is

$$M^{\rm diag} = \frac{(\gamma^{\rm diag}(0))^2}{\chi^{\rm diag}(0)} = \frac{\hbar^2}{\Gamma^2}\sum_k \left|\frac{\partial n(e)}{\partial e}\right|_{e=e_k}\left(\frac{\partial e_k}{\partial Q}\right)^2. \quad (17)$$

If the single-particle widths are properly taken into consideration, the nondiagonal contributions to the inertia are [28,29]

$$M^{\rm nondiag} = M^{\rm cr} = \hbar^2\sum_{k\neq k'}\frac{|F_{kk'}|^2}{e_{kk'}^2 + \Gamma^2}\frac{n(e_k) - n(e_{k'})}{e_{k'} - e_k}. \quad (18)$$

The main contribution to M is the diagonal part $M^{\rm diag}$ because it dominates for collective variables which are responsible for changes of the single-particle spectrum [22,32,33]. If the single-particle spectrum is almost independent of Q, $\partial e_k/\partial Q \approx 0$ and the contribution of $M^{\rm diag}$ to M is negligible. For example, at $Q = R$ and two separate nuclei $M^{\rm diag} \approx 0$ and $M^{\rm nondiag}$ is equal to the reduced mass. The overlapping of nuclei and motion to smaller R could considerably change the shell structure. In this case $M^{\rm diag}$ becomes much larger than $M^{\rm nondiag}$. The growth of the neck destroys the structure of colliding nuclei and the diagonal part dominates in the mass parameter in neck. Note that the calculation of $M^{\rm diag}$ is simpler than that of $M^{\rm nondiag}$. It was stressed in [26,37] that within the linear response theory the diagonal component of the friction parameter originates from the "heat pole" of the correlation function and vanishes when the system is ergodic. As shown in Ref. [38], the well-necked DNS-type configurations are not ergodic and stable against chaos. Even at zero excitation energy the level crossings at the Fermi surface lead to considerable mass flow [22,32,33] and the diagonal component of the correlation function (or mass parameter) does not vanish.

Taking into account only the pairing interaction, in Refs. [4,22,34] the following expression for the inertia was derived:

$$M = M^{\rm nondiag} + \hbar^2\sum_k \frac{1}{v_k^2\sqrt{e_k + \Delta^2}}\left(\frac{\partial u_k}{\partial Q}\right)^2, \quad (19)$$

where $u_k^2 = \frac{1}{2}(1 + \frac{e_k}{\sqrt{e_k^2+\Delta^2}})$, $v_k^2 = 1 - u_k^2$, and Δ defines the pairing gap. The diagonal part appears in Eq. (19). Taking into account the main contribution to the sum in Eq. (19) from the single-particle levels near the Fermi surface, the diagonal part is rewritten as

$$M^{\rm diag} \approx \frac{\hbar^2}{2\Delta^2}\sum_k \left|\frac{\partial n(e)}{\partial e}\right|_{e=e_k}\left(\frac{\partial e_k}{\partial Q}\right)^2, \quad (20)$$

where $n = v_k^2$. As seen, Eq. (20) coincides with Eq. (17) at $\Gamma = \sqrt{2}\Delta$. The presence of residual interaction (at least the paring forces) is responsible for the appearance of diagonal term in the expression for the inertia parameter.

III. CALCULATED RESULTS

A. Adiabatic two-center shell model

Because in fusion and quasifission we deal with strongly elongated systems, the two-center shell model (TCSM) [6,7,14,39–41] is appropriate for calculating the potential energy surface. In the TCSM we use the nuclear shapes are defined by the following collective coordinates: the elongation $\lambda = l/(2R_0)$ measuring the length l of the system in units of the diameter $2R_0$ of the spherical compound nucleus and used to describe the relative motion, the mass and charge asymmetry coordinates η and η_Z, respectively, the neck parameter $\varepsilon = E_0/E'$ defined by the ratio of the actual barrier height E_0 to the barrier height E' of the two-center oscillator, and the deformation parameters $\beta_i = a_i/b_i, i = 1,2$, of axially symmetric fragments, defined by the ratio of the semiaxes of the fragments. While in the cold fusion reactions we deal with almost spherical nuclei, $\beta_i \approx 1$, the heavy nuclei in the hot fusion reactions are well deformed, $\beta_i \approx 1.3$. The neck grows with decreasing ε. There is no well necked-in shape for $\lambda < 1.65$ and $\varepsilon < 0.2$.

With the TCSM the potential energy can be calculated as the sum of two terms,

$$U(\lambda,\varepsilon,\beta_i,\eta) = U_{\rm LD}(\lambda,\varepsilon,\beta_i,\eta) + U_{\rm shell}(\lambda,\varepsilon,\beta_i,\eta). \quad (21)$$

The first term is a smoothly varying macroscopic energy calculated with the liquid-drop model. The second term contains microscopic corrections which arise due to the shell structure of the nuclear system. Because of the small (not more than 15 MeV) DNS excitation energies considered, the dependence of $U_{\rm shell}$ on the temperature can be disregarded. In the cold fusion reactions only low angular momenta (<10–15) contribute [13,15–17] to the formation of evaporation residues of superheavy nuclei. Therefore, we neglect the dependence of the potential energy on the angular momentum in the reactions considered. Within the Strutinsky formalism the potential energy cannot be correctly calculated for a small neck ($\varepsilon > 0.75$) and values of λ_t corresponding to touching configurations. The reason for this is the liquid-drop energy in Eq. (21) which does not include the attractive nucleus-nucleus

potential between almost separated nuclei. Therefore, we mainly study the DNS dynamics at $\lambda \leqslant \lambda_t$ and $\varepsilon \leqslant 0.75$. In this region of collective coordinates the mass coefficients as well as the potential energy are correctly calculated.

B. Mass parameters as functions of collective coordinates

Since each single-particle state "k" has its own width Γ_k, Eq. (17) is generalized as ($Q_i = \lambda, \eta, \eta_Z, \varepsilon, \beta_1, \beta_2$)

$$M_{ij}^{\rm diag} = \hbar^2 \sum_k \frac{f_k}{\Gamma_k^2} \frac{\partial e_k}{\partial Q_i} \frac{\partial e_k}{\partial Q_j}. \tag{22}$$

For the Fermi occupation numbers $n(e_k)$, the function

$$f_k = -\frac{dn_k}{de_k} = \frac{1}{4T_0} \cosh^{-2}\left(\frac{e_k}{2T_0}\right) \tag{23}$$

has a bell-like shape with a width T_0 and is peaked at the Fermi energy. Analogously one can generalize the formula for nondiagonal mass parameters (18).

In order to calculate the width of the single-particle states, we use the well-known expression [26]

$$\Gamma_k = \frac{1}{\Gamma_0} \frac{e_k^2 + (\pi T_0)^2}{1 + \left[e_k^2 + (\pi T_0)^2\right]/c^2}. \tag{24}$$

For small excitations, Eq. (24) is reduced to the expression known in the theory of a Fermi liquid. Both parameters Γ_0 and c are known from experience with the optical model potential and the effective masses [26]. Their values are in the following ranges: $0.030\,\text{MeV}^{-1} \leqslant \Gamma_0^{-1} \leqslant 0.061\,\text{MeV}^{-1}$, $15\,\text{MeV} \leqslant c \leqslant 30\,\text{MeV}$. For the parameter c in Eq. (24) we use the "standard" value 20 MeV although the mass tensor depends quite weakly on this parameter. In the calculations we set the parameter $\Gamma_0^{-1} = 0.045\,\text{MeV}^{-1}$ in Eq. (22).

Various calculations of the mass parameters were carried out with the expressions similar to Eq. (22), for example in Refs. [4,28,33]. When the system adiabatically moves toward the compound nucleus in λ, the value of $M_{\lambda\lambda}$ approximately increases by a factor of 10–15. For the well necked-in configurations at $\lambda > \lambda_t$, $M_{\lambda\lambda} \approx \mu(\frac{\partial R}{\partial \lambda})^2$, where $\mu = m\frac{A_1 A_2}{A}$ is the reduced mass (m—the nucleon mass) and R the relative distance between the centers of nuclei. The microscopical part of potential energy remains almost unchanged when the value of λ increases from λ_t [39]. Thus, at large $\lambda > \lambda_t$, $M_{\lambda\lambda} \approx M_{\lambda\lambda}^{\rm cr}$ and $M_{\lambda\lambda}^{\rm diag} = 0$. In Fig. 1, one can see the dependence of $M_{\lambda\lambda} = M_{\lambda\lambda}^{\rm diag} + M_{\lambda\lambda}^{\rm cr}$ on λ and ε in the case of the ^{64}Ni + ^{208}Pb reaction. The inhomogeneities of this dependence are caused by the shell effects. The value of $M_{\lambda\lambda}$ grows stronger with decreasing λ at large ε than at small ε. At $\lambda = 1.5$–1.55 the value of $M_{\lambda\lambda}$ is almost constant at $0.4 < \varepsilon < 0.8$ and grows at smaller ε.

The dependence of $M_{\varepsilon\varepsilon}$ on λ and ε is presented in Fig. 2 for the ^{64}Ni + ^{208}Pb system. The obtained values of $M_{\varepsilon\varepsilon} = M_{\varepsilon\varepsilon}^{\rm diag} + M_{\varepsilon\varepsilon}^{\rm cr}$ have the same order of magnitude as in Ref. [17]. However, due to the larger shell effect in the entrance channel of cold fusion reaction because of the doubly magic ^{208}Pb, the mass parameter in neck becomes about two times larger (at the same fixed T_0) than that in the case of symmetric reactions like ^{110}Pd + ^{110}Pd [14]. At

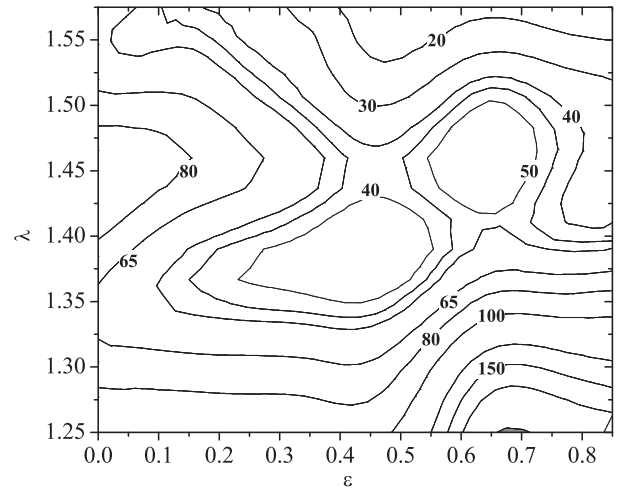

FIG. 1. The calculated mass parameter $M_{\lambda\lambda}$ in units $10^3 m$ fm^2 as a function of λ and ε in the ^{64}Ni + ^{208}Pb reaction.

λ corresponding to touching configuration the value of $M_{\varepsilon\varepsilon}$ increases by about a factor of 5 when ε decreases from 0.8 to 0. This increase is related to the decrease of the shell correction $U_{\rm shell}$ with ε toward $\varepsilon \to 0$. Smaller values of $U_{\rm shell}$ correspond to larger mass parameters. At $\lambda < 1.4$ the value of $M_{\varepsilon\varepsilon}$ is almost independent of ε. Because at small λ the shape of the system weakly depends on ε and the potential energy is rather flat function of ε, the value of $M_{\varepsilon\varepsilon}$ decreases with λ.

Comparing our results of M_{ij} with M_{ij}^{WW} obtained in the Werner-Wheeler approximation for a touching configuration, we find $M_{\lambda\lambda} = M_{\lambda\lambda}^{WW}$, $M_{\varepsilon\varepsilon} \approx 50 M_{\varepsilon\varepsilon}^{WW}$, $M_{\lambda\varepsilon} \approx 0.4 M_{\lambda\varepsilon}^{WW}$, and $M_{\lambda\varepsilon}/\sqrt{M_{\lambda\lambda} M_{\varepsilon\varepsilon}} \ll 1$ in the cold fusion reactions considered. Therefore, we can conclude that the microscopical mass parameter of the neck is much larger than the one in the Werner-Wheeler approximation and the nondiagonal component $M_{\lambda\varepsilon}$ is small to be disregarded in the dynamical calculations. The choice of the width is crucial for the value of $M^{\rm diag}$ in both the diabatic and adiabatic cases within a reasonable

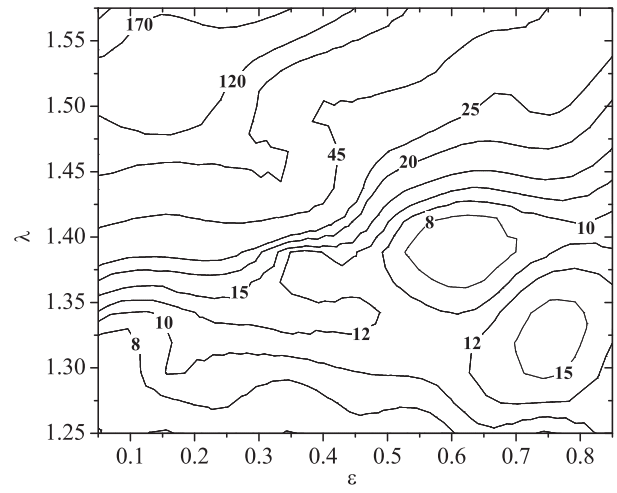

FIG. 2. The calculated mass parameter $M_{\varepsilon\varepsilon}$ in units $10^3 m$ fm^2 as a function of λ and ε in the ^{64}Ni + ^{208}Pb reaction.

variation. If instead of $\Gamma_0^{-1} = 0.045$ MeV^{-1} the value of Γ_0^{-1} is taken as 0.03 MeV^{-1} at the lower limit, the value of $M_{\varepsilon\varepsilon}$ becomes 2.25 times smaller, but remains larger than $M_{\varepsilon\varepsilon}^{WW}$ by about 20 times. For larger temperatures, the average width Γ increases and the function f_k/Γ_k^2 becomes smoother. The mass parameter $M_{\varepsilon\varepsilon}$ depends on temperature T_0 mainly due to the width Γ_k of the single-particle levels ($\Gamma_k \sim T_0^2$). The value of $M_{\varepsilon\varepsilon}$ decreases with T_0^{-4}. One- and two-body interactions [29] contribute to the nondiagonal and diagonal parts of the mass parameter $M_{\varepsilon\varepsilon}$, respectively. Whereas the one-body nondiagonal contribution to the mass is relatively insensitive to the temperature of system, the diagonal two-body contribution increases strongly with decreasing temperature. So, $M_{\varepsilon\varepsilon}^{\rm diag}(T_0 = 1.0\,{\rm MeV})/M_{\varepsilon\varepsilon}^{\rm diag}(T_0 = 1.5\,{\rm MeV}) \sim 5.2$ which is shown in Fig. 7. We found the largest contribution of the two-body component to the neck mass parameter already at a quite high excitation energy of 30 MeV ($T_0 = 1.3$ MeV) of the DNS in fusion reactions [17]. For comparison, the excitation energies of the initial DNS in Pb- and Bi-based cold fusion reactions are smaller than 20 MeV ($T_0 < 1.0$ MeV). So, the value of $M_{\varepsilon\varepsilon}$ is not crucial to T_0 in these reactions.

Because at the touching configuration the slope of the single-particle levels is small, the microscopical mass parameter in λ is close to its smooth, hydrodynamical value. In contrast, a large amount of internal reorganization occurs at the level crossings with decreasing ε and leads to a large neck inertia of the initial DNS. So, the value of $M_{\varepsilon\varepsilon}$ exceeds the mass in the hydrodynamical model due to large values of $|\partial e_k/\partial\varepsilon|$. The restriction for the growth of the neck may be understood by analyzing the single-particle spectrum as a function of ε [14]. Well necked-in shapes with large ε have single-particle spectra with a good shell structure. The spectra show a larger number of level crossings with increasing ε. Finally, we should stress that the mass parameter in neck remains always much larger in fusion reactions than the mass calculated with the hydrodynamical Werner-Wheeler approximation.

C. Parametrizations for the mass parameters

Calculating the mass parameters for cold fusion reactions ^{48}Ca, ^{50}Ti, ^{54}Cr, ^{58}Fe, ^{64,72,78}Ni, ^{70}Zn + ^{208}Pb [1], one can suggest the following parametrizations for the mass parameters as functions of λ and ε:

$$M_{\lambda\lambda} \approx \mu_\lambda\left(1 + 274.9\frac{N-Z}{A} \times \exp\left[(\lambda_t - \lambda)(1+9\varepsilon) - 11.9\frac{N-Z}{A}\right]\right), \quad (25)$$

where $\mu_\lambda = (2R_0)^2\mu$, $A = A_1 + A_2$, $N = N_1 + N_2$, and $Z = Z_1 + Z_2$ are the mass, neutron, and proton numbers of the DNS, respectively, and

$$M_{\varepsilon\varepsilon} \approx B(\lambda) + \frac{f(\lambda)}{1 + v(\lambda)\exp[9.09\varepsilon]} \quad (26)$$

with

$$B(\lambda) = 617 - 930\lambda + 354\lambda^2$$

and

$$f(\lambda) = 200 + \frac{208}{1 + \exp[20(\lambda - 1.46)]}$$

in units of $10^3 m$ fm^2, and

$$v(\lambda) = \exp\left[9.09\left(0.89 - 0.16\frac{A}{N-Z}\lambda\right)\right].$$

In the parametrization (26) of the mass coefficient $M_{\varepsilon\varepsilon}$ as a function of λ and ε, we obtain $B = 26.36 \times 10^3 m$ fm^2, $f = 230 \times 10^3 m$ fm^2, and $v = 0.02$ for the reactions considered. In this case

$$\frac{\partial M_{\varepsilon\varepsilon}}{\partial\varepsilon} \approx \frac{\alpha f}{v}\exp[-\alpha\varepsilon]. \quad (27)$$

D. Dynamics of DNS in potential energy surface

In this paper we concentrate on the role of the mass parameter $M_{\varepsilon\varepsilon}$ in the motion of the neck coordinate to test whether the DNS exists with a relatively small neck during sufficient time. For almost head-on collisions the classical collective kinetic energy is given as

$$T = \frac{1}{2}\sum_{i,j} M_{ij}(Q)\dot{Q}_i\dot{Q}_j, \quad (28)$$

where M_{ij} ($i, j =$ "λ","ε", $Q_\lambda = \lambda$ and $Q_\varepsilon = \varepsilon$) are the shape-dependent mass parameters. The dissipative forces are included with the Rayleigh dissipation function

$$\Phi = \frac{1}{2}\sum_{i,j}\gamma_{ij}(Q)\dot{Q}_i\dot{Q}_j, \quad (29)$$

where for simplicity the friction coefficients γ_{ij} are calculated with the expression

$$\gamma_{ij} = \Gamma M_{ij}/\hbar \quad (30)$$

following the linear response theory [26]. The quantity $\Gamma = 2$ MeV is consistent with Refs. [42–44]. The dynamics of the nuclear shape is obtained by solving the equations of motion resulting from the Lagrangian $L = T - U$ and the Rayleigh dissipation function Φ.

In order to obtain the correct potential energy, as in the DNS model, for the touching configuration, in the TCSM the neck parameter ε should be set about 0.75 [14]. With this value of ε the neck radius and the distance between the centers of the nuclei are approximately equal to the corresponding quantities in the DNS.

The calculated potential energies in (λ,ε) space are presented in Figs. 3 an 4 for the reactions ^{64}Ni + ^{208}Pb and ^{70}Zn + ^{208}Pb. In these reactions the touching configurations correspond to $\lambda = \lambda_t = 1.53$–$1.54$ and $\varepsilon = \varepsilon_t = 0.75$. At $1.25 < \lambda < 1.45$ the shell effects shift the position of potential minimum from $\varepsilon = 0$ toward larger ε. Therefore, the fission-type valley along λ (the minimum of potential energy as a function of ε at given λ) corresponds to $\varepsilon = 0$ at $\lambda > 1.5$, $\varepsilon = 0.4$ at $1.4 < \lambda < 1.5$, and $0.1 < \varepsilon < 0.4$ at $1.25 < \lambda < 1.4$.

Because of the shell effects related to the doubly magic ^{208}Pb in the cold fusion reactions, the gradient of the potential to smaller ε is smaller than that in the case of symmetric fusion

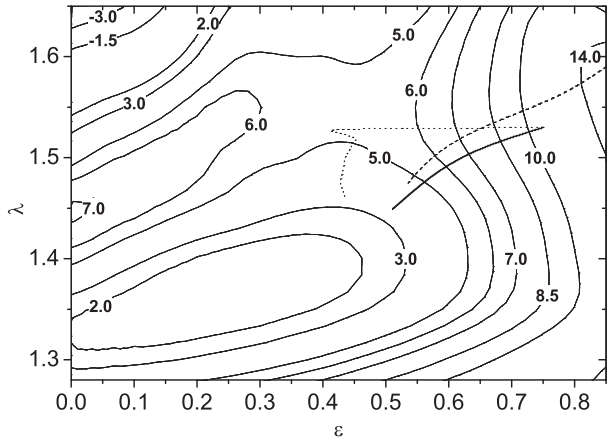

FIG. 3. Contours of the potential energy surface, in units of MeV, calculated in the (λ,ε) plane for the ^{64}Ni + ^{208}Pb reaction. The potential energy is with respect to the liquid-drop energy of the spherical compound nucleus. The dynamical trajectories are calculated at $\lambda(0) = 1.53$, $\varepsilon(0) = 0.75$ (solid line) and $\lambda(0) = 1.59$, $\varepsilon(0) = 0.85$ (dashed line) with microscopic mass coefficients. The dynamical trajectory calculated at $\lambda(0) = 1.53$, $\varepsilon(0) = 0.75$ with the Werner-Wheeler masses is presented by a dotted line. The initial kinetic energy is zero for all trajectories shown.

reactions [14]. Also the position of potential-energy minimum at $\lambda < \lambda_t$ can strongly deviate from $\varepsilon = 0$. Thus, the adiabatic potential surface is not in favor of the fast growth of neck at $1.4 < \lambda < \lambda_t$. As in Ref. [41], the strong shell effects are related to the certain neck size. In the ^{208}Pb- and ^{209}Bi-based complete fusion reactions with almost spherical nuclei, the fusioning system is in the potential minimum in η due to the strong shell effect. So, the value of η and deformations can be

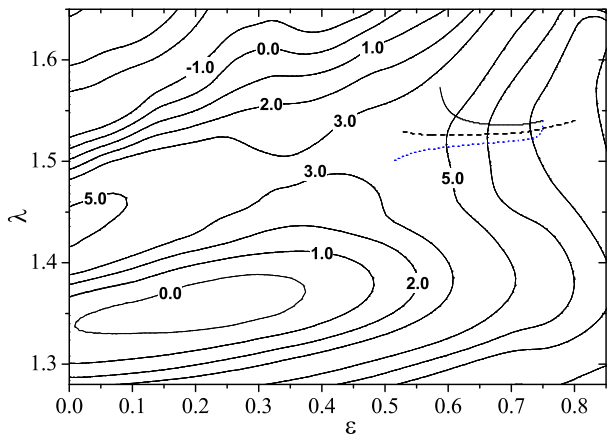

FIG. 4. (Color online) Contours of the potential energy surface, in units of MeV, calculated in the (λ,ε) plane for the ^{70}Zn + ^{208}Pb reaction. The potential energy is with respect to the liquid-drop energy of the spherical compound nucleus. The dynamical trajectories are calculated at $\lambda(0) = 1.53$, $\varepsilon(0) = 0.75$ (solid line) and $\lambda(0) = 1.53$, $\varepsilon(0) = 0.8$ (dashed line) with microscopic mass coefficients and zero initial kinetic energy. The dynamical trajectory calculated at $\lambda(0) = 1.53$, $\varepsilon(0) = 0.75$ with microscopic mass coefficients and 1 MeV initial kinetic energy is presented by dotted line.

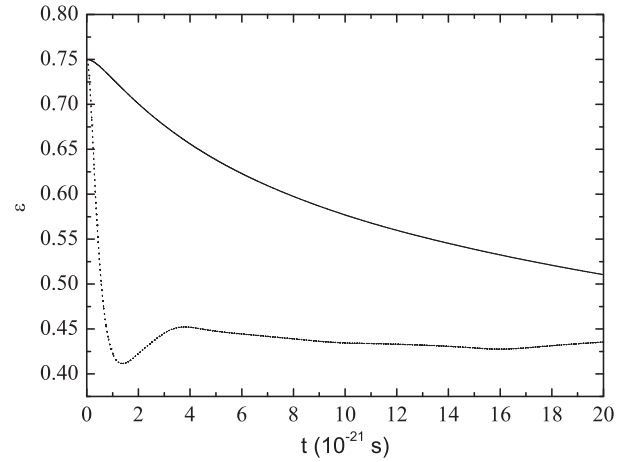

FIG. 5. Time-dependence of the neck parameter ε in the ^{64}Ni + ^{208}Pb reaction calculated with microscopic (solid line) and Werner-Wheeler (dotted line) mass parameters. The initial conditions are $\lambda(0) = 1.53$, $\varepsilon(0) = 0.75$, and zero kinetic energy.

taken fixed and only the dynamics in λ (or R) and ε has to be considered.

The calculated DNS trajectories on the potential energy surfaces are shown in Figs. 3 an 4. As seen, with microscopical mass parameters the system remains with rather long time near the entrance configuration. In 2×10^{-20} s, which exceeds the characteristic time of complete fusion, the value of ε decreases only from 0.75 till about 0.5–0.6. The change of the initial conditions leads to other trajectory which, however, comes in about 10^{-20} s to the same region of (λ,ε) plane. Thus, the main conclusion about the long-living DNS configuration coming from our dynamical calculation is rather insensitive to the reasonable variation of initial conditions.

While being considered with the microscopical mass parameters, the system does not reach the fission-type valley in 2×10^{-20} s, it falls into this valley in 10^{-21} s if the mass parameters are taken in the Werner-Wheeler approximation. The trajectory obtained with the Werner-Wheeler masses is presented in Fig. 3. Time-dependence of the neck parameter along the trajectories calculated with the microscopical and Werner-Wheeler mass formulas are compared in Fig. 5. One can see the fast decrease of ε (the increase of neck size) in the liquid-drop approximation, where the DNS dynamics is mainly ruled by only potential energy surface. In the microscopical approach the neck growths very slowly and the system remains close to the entrance channel. So, in the microscopical consideration the mass tensor strongly affects the dynamics.

The same can be also concluded from the dynamics of more asymmetric system ^{48}Ca + ^{208}Pb (Fig. 6). Because of the strong shell effects in these two doublly magic nuclei, the microscopical mass parameter $M_{\varepsilon\varepsilon}$ is much larger than that in the Werner-Wheeler approach. This causes a quite small change of neck in 2×10^{-20} s. With the hydrodynamical masses the system would instantly fall into the fission-type valley and evolves there to the compound nucleus on the way to which there is no potential barrier. In Fig. 7 the contours of the potential energy surface are presented for the ^{78}Ni + ^{208}Pb reaction. As seen, the potential energy prevents the motion to smaller λ,

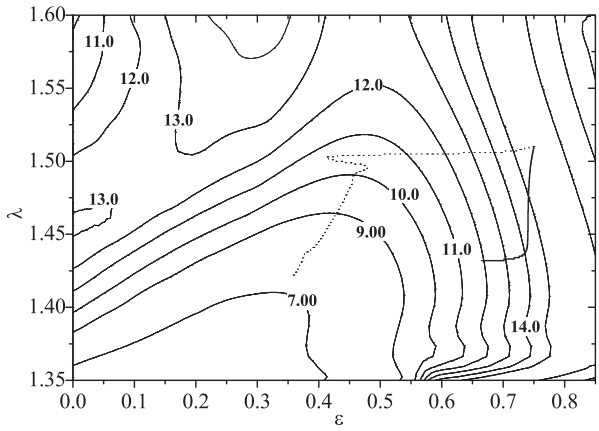

FIG. 6. Contours of the potential energy surface, in units of MeV, calculated in the (λ,ε) plane for the $^{48}\mathrm{Ca}+{}^{208}\mathrm{Pb}$ reaction. The potential energy is with respect to the liquid-drop energy of the spherical compound nucleus. The dynamical trajectories are calculated at $\lambda(0)=1.51$, $\varepsilon(0)=0.75$ with microscopic mass coefficients (solid line) and with the Werner-Wheeler masses (dotted line). The initial kinetic energy is zero for all trajectories shown.

i.e., the fusion being considered as an adiabatic melting in λ is suppressed with increasing neutron number in the projectile of cold fusion reactions. Comparing Figs. 3, 4, 6, and 7 we can conclude that the system is easily captured into the potential valley at smaller $Z_1 \times Z_2$ and smaller number of neutrons.

E. Effect of dependence of $M_{\varepsilon\varepsilon}$ on ε

In order to show analytically the influence of the increase of $M_{\varepsilon\varepsilon}$ with decreasing ε on the neck dynamics, one can write the one-dimensional equation of motion in ε

$$M_{\varepsilon\varepsilon}\ddot{\varepsilon} = -\frac{\partial U}{\partial \varepsilon} - \frac{\dot{\varepsilon}^2}{2}\frac{\partial M_{\varepsilon\varepsilon}}{\partial \varepsilon}. \tag{31}$$

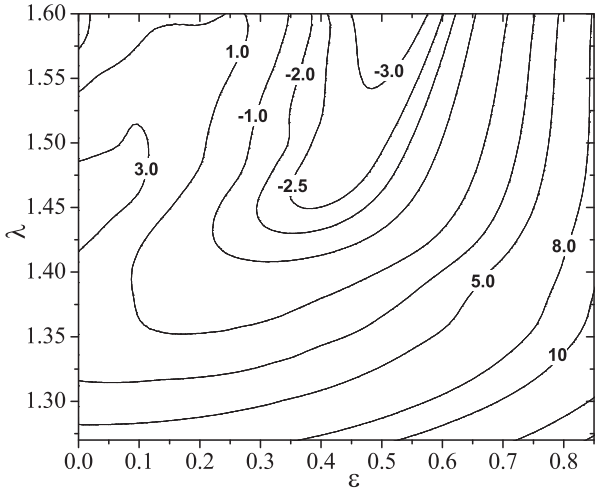

FIG. 7. Contours of the potential energy surface, in units of MeV, calculated in the (λ,ε) plane for the $^{78}\mathrm{Ni}+{}^{208}\mathrm{Pb}$ reaction. The potential energy is with respect to the liquid-drop energy of the spherical compound nucleus.

The effect of friction is disregarded here and will be considered below. At $\dot{\varepsilon}(0)=0$, Eq. (31) is rewritten as

$$M_{\varepsilon\varepsilon}\ddot{\varepsilon} = -\frac{\partial U}{\partial \varepsilon} - (U_t - U)\frac{1}{M_{\varepsilon\varepsilon}}\frac{\partial M_{\varepsilon\varepsilon}}{\partial \varepsilon}. \tag{32}$$

Here U_t is the potential energy of the initial DNS with $\varepsilon=\varepsilon_t$ at $\lambda=\lambda_t$. Taking into consideration Eqs. (26) and (27) and approximating the potential energy by the linear function of ε,

$$U(\varepsilon) \approx U_t + \beta(\varepsilon_t - \varepsilon), \tag{33}$$

we obtain

$$M_{\varepsilon\varepsilon}\ddot{\varepsilon} \approx -\frac{\partial U}{\partial \varepsilon} + \alpha\beta(\varepsilon_t - \varepsilon) = \frac{\partial}{\partial \varepsilon}\left[U + \frac{\alpha\beta}{2}(\varepsilon_t - \varepsilon)^2\right]. \tag{34}$$

Because α and β are positive, the dependence of $M_{\varepsilon\varepsilon}$ on ε effectively leads to the additional potential which partly compensates the decrease of U. Thus, the absolute value of the gradient of potential becomes smaller and the neck grows with smaller rate.

In the case of nonzero friction coefficient γ at quite small time

$$\frac{M_{\varepsilon\varepsilon}\dot{\varepsilon}^2}{2} \approx U_t - U - \gamma\bar{\dot{\varepsilon}}(\varepsilon_t - \varepsilon) = (\beta - \gamma\bar{\dot{\varepsilon}})(\varepsilon_t - \varepsilon), \tag{35}$$

where $\bar{\dot{\varepsilon}}$ is the average velocity in the interval between ε_t and ε. As seen, the friction effectively decreases the value of β. So, the effects of $M_{\varepsilon\varepsilon}(\epsilon)$ and friction on the rate of neck growth are opposite. However, in the vicinity of ε_t the value of $\dot{\varepsilon}$ is rather small due to quite large $M_{\varepsilon\varepsilon}$ and the coordinate dependence of $M_{\varepsilon\varepsilon}$ mainly influences the neck dynamics. It promotes small change of ε and long-living DNS configuration.

F. Complete fusion probability with adiabatic potential

An adiabatic potential energy surface is used in our calculations. Because there are no suitable potential barriers in it which hinders a growth of the neck, the neck parameter decreases steadily to smaller values, faster in the case with the Werner-Wheeler mass parameters, and much slower with the microscopical mass parameters. Therefore, one has to explore whether at almost fixed ε an adiabatic melting of nuclei in λ can explain the experiments on the cold fusion [14].

The potential energies as functions of λ at fixed ε are presented in Fig. 8 for the systems formed in cold fusion reactions $^{48}\mathrm{Ca}$, $^{50}\mathrm{Ti}$, $^{54}\mathrm{Cr}$, $^{58}\mathrm{Fe}$, $^{64}\mathrm{Ni}$, $^{70}\mathrm{Zn}+{}^{208}\mathrm{Pb}$. The touching configurations correspond to $\lambda=\lambda_t=1.51$–1.54. The position of the outer barrier, which keeps the system against a decay in λ, corresponds to larger values of λ. So, after touching the system slides in the potential minimum at almost fixed ε. The melting in λ would compete in this case with the decay over the outer barrier. Denoting the height of the inner barrier by B_λ and the height of the outer barrier by B^λ_{qf}, one can estimate the fusion probability in λ as

$$P^\lambda_{\mathrm{CN}} \sim \exp\left[\left(B_\lambda - B^\lambda_{\mathrm{qf}}\right)/T_0\right].$$

If there is no outer barrier, then in this expression we take $U(\lambda_t)$ instead of B^λ_{qf}.

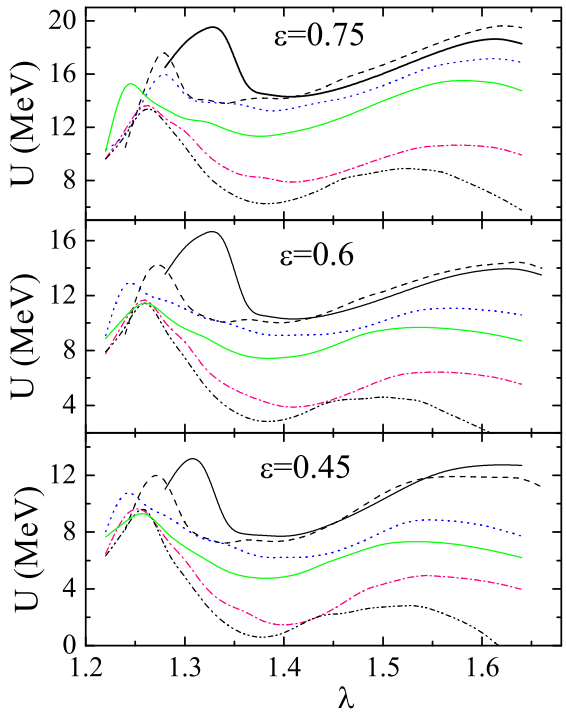

FIG. 8. (Color online) Potentials as functions of elongation λ at indicated values of ε in the systems ^{48}Ca + ^{208}Pb (solid lines), ^{50}Ti + ^{208}Pb (dashed lines), ^{54}Cr + ^{208}Pb (dotted lines), ^{58}Fe + ^{208}Pb (thick solid lines), ^{64}Ni + ^{208}Pb (dash-dotted lines), and ^{70}Zn + ^{208}Pb (dash-dot-dotted lines). The potential energy is with respect to the liquid-drop energy of the corresponding spherical compound nucleus.

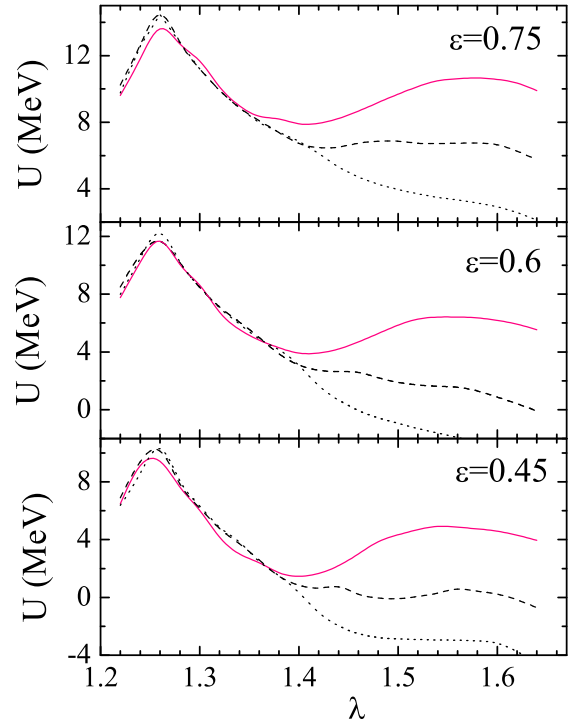

FIG. 9. (Color online) The same as in Fig. 8, but for the systems ^{64}Ni + ^{208}Pb (solid lines), ^{72}Ni + ^{208}Pb (dashed lines), and ^{78}Ni + ^{208}Pb (dotted lines).

One can see in Fig. 8 that the fusion probability $P_{\rm CN}$, which depends on the difference of the heights of the inner and outer barriers, would be larger in the the reactions ^{50}Ti, ^{54}Cr, ^{58}Fe + ^{208}Pb than in the ^{48}Ca + ^{208}Pb reaction at $\varepsilon = 0.6$ and 0.75. At $\varepsilon = 0.45$ the fusion probability in the ^{48}Ca + ^{208}Pb reaction is expected to be smaller than in the ^{50}Ti + ^{208}Pb reaction. At $\varepsilon = 0.45$ and 0.6 the fusion probabilities in the reactions ^{54}Cr, ^{58}Fe + ^{208}Pb are expected to be close. However, the DNS model [15] provides the difference of about 30 times to explain the experimental data. While the fusion probability in the ^{58}Fe + ^{208}Pb reaction should be 3–5 times larger than in the ^{64}Ni + ^{208}Pb reaction [15], the potentials in Fig. 8 show the results of the difference of more than 30 times. The ratio of the fusion probabilities in the reactions ^{64}Ni, ^{70}Zn + ^{208}Pb, which is about 10 [15], seems to be correctly described with the potentials at $\varepsilon = 0.45$ and 0.6 in Fig. 8. So, in most cases the adiabatic potential energy surface causes the problems in describing the fusion probabilities in the cold fusion reactions. In the ^{50}Ti + ^{208}Pb reaction, the adiabatic potential provides $B_\lambda - B^\lambda_{\rm qf} < 0$ that cannot be consistent with the experimental data.

As follows from the potentials in Fig. 9, in the reactions ^{64,72,78}Ni + ^{208}Pb the fusion probability in λ decreases with increasing mass number of the projectile. There are no good potential minima near the touching configuration in the reactions ^{72,78}Ni + ^{208}Pb. This causes quite a fast decay in λ. The ratio of the fusion probabilities in the reactions ^{64,72}Ni + ^{208}Pb is estimated as 6×10^3 with the potentials in Fig. 9 while it is about 2×10^2 in the DNS model. So, the adiabatic melting in λ results in a much stronger isotopic dependence of the fusion probability than in the DNS model which describes well many complete fusion reactions.

G. Role of diabatic effects in complete fusion

Besides the microscopic mass parameters, the transition between diabatic and adiabatic regimes has to be taken into account in the consistent consideration of fusion because the fusion time is rather short [17,19,45]. The diabatic effect might additionally restrict the neck growth and the motion to smaller λ [17,45]. Therefore, the dynamical calculations with the adiabatic potential energy $U = U_{\rm ad}$ show a maximum possible growth of the neck. The time-dependent potential

$$U(t) = U_{\rm ad} + (U_d - U_{\rm ad})e^{-t/\tau}, \tag{36}$$

where U_d is diabatic potential, τ characterizes the transient time from diabatic regime to adiabatic limit. As in Ref. [19], the value of τ is estimated as

$$\tau = \frac{2\hbar}{\langle\Gamma\rangle}, \tag{37}$$

where $\langle\Gamma\rangle$ is an average single-particle width near the Fermi surface. Because $U_{\rm ad}(\varepsilon \approx 0.75) - U_{\rm ad}(\varepsilon = 0)$ at $\lambda = \lambda_t$ is about 10 MeV in the reactions treated, and U_d could exceed $U_{\rm ad}$ by about 100 MeV, the value of τ must be larger than 2×10^{-21} s to get at least flat potential U at interaction time $t \approx 8 \times 10^{-21}$ s. The rough estimate with Eq. (37) gives the

values of τ just close to 2×10^{-21} s. Thus, the diabatic effect additionally prohibits the neck growth.

IV. SUMMARY

Mass parameters for the relevant collective variables of the systems formed in cold fusion reactions were evaluated with the two-center shell model. Formulas for the mass parameters were derived within the linear response theory by taking the fluctuation-dissipation theorem and the width of single-particle states into account. The obtained mass parameter for the neck degree of freedom is much larger than the one obtained in the hydrodynamical model with the Werner-Wheeler approximation. By applying the microscopic mass parameters we found a relatively stable neck during the time of cold fusion reaction. So, the complete fusion in the ^{208}Pb-based reactions occurs at almost fixed neck parameter ε. In addition the diabatic or structural forbiddenness effect hinders the motion to smaller internuclear distances and larger neck size. Therefore, the DNS configuration exists for a sufficiently long time, comparable with the characteristic time of complete fusion, that is just assumed in the DNS model of fusion. If one tries to describe fusion as a melting with adiabatic potential surface and realistic mass parameters, then incorrect ratios of fusion probabilities could come out for neighboring cold fusion reactions. Our results could also support the existence of long-living cluster configurations.

The cold fusion reactions considered contain magic ^{208}Pb. As a result, the neck growth leads to the strong change of nuclear structure and the mass parameter in ε is quite large. In the case of hot fusion actinide-based reactions the shell effects are weaker in the entrance channel and the mass parameter in ε is expected to be smaller than those presented in the paper. However, its value is still enough to prevent the fast growth of the neck.

ACKNOWLEDGMENTS

We are thankful to Werner Scheid for useful discussions. G.G.A. and N.V.A. are grateful for support of the Alexander von Humboldt-Stiftung (Bonn). This work was supported in part by RFBR (Moscow).

[1] S. Hofmann and G. Münzenberg, Rev. Mod. Phys. **72**, 733 (2000).
[2] Yu. Ts. Oganessian, J. Phys. G **34**, R165 (2007).
[3] P. G. Thirolf and D. Habs, Prog. Part. Nucl. Phys. **49**, 325 (2002).
[4] M. Brack, J. Damgaard, A. S. Jensen, H. C. Pauli, V. M. Strutinsky, and C. Y. Wong, Rev. Mod. Phys. **44**, 320 (1972).
[5] G. D. Adeev, I. A. Gamalya, and P. A. Cherdantsev, Sov. J. Nucl. Phys. **12**, 148 (1971); Bull. Acad. Sci. USSR, Phys. **36**, 583 (1972).
[6] J. Maruhn and W. Greiner, Z. Phys. A **251**, 431 (1972).
[7] J. Maruhn, W. Scheid, and W. Greiner, in *Heavy Ion Collisions*, edited by R. Bock (North-Holland, Amsterdam, 1980), Vol. 2, p. 397.
[8] W. J. Swiatecki, Phys. Scr. **24**, 113 (1981).
[9] V. V. Volkov, Phys. Rep. **44**, 93 (1978); *Deep Inelastic Nuclear Reactions* (Energoizdat, Moscow, 1982).
[10] V. V. Volkov, Izv. AN SSSR Ser. Fiz. **50**, 1879 (1986); in *Proceedings of the International Conference on Nuclear Reaction Mechanisms, Varenna, 1991*, edited by E. Gadioli (Milano Univ. degli Studi di Milano, Milano, 1991), p. 39.
[11] P. Fröbrich, Phys. Rep. **116**, 337 (1984).
[12] W. U. Schröder and J. R. Huizenga, in *Treatise on Heavy-Ion Science*, edited by D. A. Bromley (Plenum, New York, 1984), Vol. 2, p. 115; V. V. Volkov, *Treatise on Heavy-Ion Science* (Plenum Press, New York, 1989), Vol. 8, p. 101.
[13] N. V. Antonenko, E. A. Cherepanov, A. K. Nasirov, V. P. Permjakov, and V. V. Volkov, Phys. Lett. B **319**, 425 (1993); Phys. Rev. C **51**, 2635 (1995); G. G. Adamian, N. V. Antonenko, and W. Scheid, Nucl. Phys. A **618**, 176 (1997); G. G. Adamian, N. V. Antonenko, W. Scheid, and V. V. Volkov, *ibid.* **627**, 361 (1997); **633**, 409 (1998); R. V. Jolos, A. K. Nasirov, and A. I. Muminov, Eur. Phys. J. A **4**, 245 (1999); E. A. Cherepanov, Pramana **23**, 1 (1999); V. V. Volkov, Part. and Nucl. **35**, 797 (2004).
[14] G. G. Adamian, N. V. Antonenko, S. P. Ivanova, and W. Scheid, Nucl. Phys. A **646**, 29 (1999).
[15] G. G. Adamian, N. V. Antonenko, and W. Scheid, Nucl. Phys. A **678**, 24 (2000).
[16] G. G. Adamian, N. V. Antonenko, and W. Scheid, in *Clusters in Nuclei*, edited C. Beck (Springer-Verlag, Berlin/Heidelberg, 2012), Vol. 2; Lecture Notes in Physics **848**, 165 (2012).
[17] G. G. Adamian, N. V. Antonenko, A. Diaz-Torres, and W. Scheid, Nucl. Phys. A **671**, 233 (2000).
[18] G. G. Adamian, N. V. Antonenko, and Yu. M. Tchulvil'sky, Phys. Lett. B **451**, 289 (1999).
[19] A. Diaz-Torres, G. G. Adamian, N. V. Antonenko, and W. Scheid, Phys. Lett. B **481**, 228 (2000).
[20] Yu. F. Smirnov and Yu. M. Tchulvil'sky, Phys. Lett. B **134**, 25 (1984).
[21] G. Bertsch, *Frontiers and Borderlines in Many-Particles Physics*, Enrico Fermi School (CIV, Corso, 1988), p. 41.
[22] W. Greiner and J. A. Maruhn, *Nuclear Models* (Springer-Verlag, Berlin/Heidelberg, 1996).
[23] R. A. Gherghescu and D. N. Poenaru, Phys. Rev. C **72**, 027602 (2005).
[24] G. G. Adamian, N. V. Antonenko, and R. V. Jolos, Nucl. Phys. A **584**, 205 (1995).
[25] J. Richert, T. Sami, and H. A. Weidenmüller, Phys. Rev. C **26**, 1018 (1982).
[26] H. Hofmann, Phys. Rep. **284**, 137 (1997).
[27] F. A. Ivanyuk, H. Hofmann, V. V. Pashkevich, and S. Yamaji, Phys. Rev. C **55**, 1730 (1997).
[28] V. Schneider, J. Maruhn, and W. Greiner, Z. Phys. A **323**, 111 (1986).
[29] S. Yamaji *et al.*, J. Phys. G **3**, 1283 (1977).
[30] D. N. Poenaru and R. A. Gherghescu, J. Phys. G **41**, 125104 (2014).
[31] A. Lukasiak, W. Cassing, and W. Nörenberg, Nucl. Phys. A **426**, 181 (1984).

[32] J. R. Primack, Phys. Rev. Lett. **17**, 539 (1966).
[33] J. J. Griffin, Nucl. Phys. A **170**, 395 (1971).
[34] T. Lederberger and H. C. Pauli, Nucl. Phys. A **207**, 1 (1973).
[35] V. M. Kolomietz and P. J. Siemens, Nucl. Phys. A **314**, 141 (1979).
[36] S. Yamaji, F. A. Ivanyuk, and H. Hofmann, Nucl. Phys. A **612**, 1 (1997).
[37] H. Hofmann *et al.*, Nucl. Phys. A **598**, 187 (1996).
[38] X. Wu, J. Gu, Y. Zhuo, Z. Li, Y. Chen, and W. Greiner, Phys. Rev. Lett. **79**, 4542 (1997).
[39] D. N. Poenaru, W. Greiner, and R. A. Gherghescu, J. Phys. G **24**, L23 (1998).
[40] R. A. Gherghescu, Phys. Rev. C **67**, 014309 (2003).
[41] R. A. Gherghescu, D. N. Poenaru, and W. Greiner, Phys. Rev. C **78**, 024604 (2008).
[42] G. G. Adamian, R. V. Jolos, A. K. Nasirov, and A. I. Muminov, Phys. Rev. C **56**, 373 (1997).
[43] K. Washiyama, D. Lacroix, and S. Ayik, Phys. Rev. C **79**, 024609 (2009); K. Washiyama, S. Ayik, and D. Lacroix, *ibid.* **80**, 031602(R) (2009).
[44] K. Wen, F. Sakata, Z. X. Li, X. Z. Wu, Y. X. Zhang, and S. G. Zhou, Phys. Rev. Lett. **111**, 012501 (2013); Phys. Rev. C **90**, 054613 (2014).
[45] A. Diaz-Torres, N. V. Antonenko, and W. Scheid, Nucl. Phys. A **652**, 61 (1999).